Hybrid 3D T1-weighted gradient-echo sequence for fiducial marker detection and tumor delineation via magnetic resonance imaging in liver stereotactic body radiation therapy

Yutaka Kato[1*], Takeshi Kamomae[2], Motoki Kumagai[2], Yumi Oie[2], Yumiko Noguchi[1], Kuniyasu Okudaira[1], Mariko Kawamura[2], Toshiaki Taoka[2], Shinji Naganawa[2]

[1]Department of Radiological Technology, Nagoya University Hospital

[2]Department of Radiology, Nagoya University Graduate School of Medicine

*Corresponding author,

Department of Radiological Technology, Nagoya University Hospital, 65 Tsurumai-cho, Shouwa-ku, Nagoya, Aichi 466-8560, Japan

Phone: +81-52-744-2566, Fax: +81-52-744-2559

E-mail: ykato@med.nagoya-u.ac.jp

Abstract

Purpose: Gold fiducial markers are used to guide liver stereotactic body radiation therapy (SBRT) and are hard to detect by magnetic resonance imaging (MRI). In this study, the parameters of the three-dimensional T1-weighted turbo gradient-echo (3D T1W-GRE) sequence were optimized for gold marker detection without degrading tumor delineation.

Methods: Custom-made phantoms mimicking tumor and normal liver parenchyma were prepared and embedded with a gold marker. The 3D T1W-GRE was scanned by varying echo time (TE), bandwidth (BW), flip angle (FA), and base matrix size. The signal-to-noise ratio (SNR), contrast ratio (CR), and relative standard deviation (RSD) of the signal intensity in the area including the gold marker were evaluated, and the parameters were optimized accordingly. The modified 3D T1W-GRE (called HYBRID) was compared with the conventional T1W-GRE- and T2*-sequences in both phantom and clinical studies. In the clinical study of six patients with primary liver tumors, two observers visually assessed marker detection, tumor delineation, and overall image quality on a four-point scale.

Results: In the phantom study, HYBRID showed significantly higher SNR and RSD than those of conventional T1W-GRE ($P < 0.001$). In the clinical study, HYBRID yielded significantly higher scores than conventional T1W-GRE did in terms of marker detection ($P < 0.001$). The scores of both sequences were not statistically different in terms of tumor delineation and overall image quality ($P = 0.56$ and $P = 0.32$).

Conclusions: The proposed HYBRID sequence improved gold fiducial marker detection without

degrading tumor delineation in MRI for SBRT of primary liver tumor.

Keywords: Liver stereotactic body radiation therapy; Gold fiducial marker; Marker detection; EOB-MRI

Introduction

The standard curative treatment for primary and metastatic liver tumors is surgery. However, radiofrequency ablation, transcatheter arterial chemoembolization, and radiotherapy are powerful alternative approaches for inoperable cases. In recent years, stereotactic body radiation therapy (SBRT) has been increasingly used for treating liver tumors, a development supported by high local control rates with acceptable toxicity [1–3]. Furthermore, the success of highly conformal radiotherapy in sparing normal tissues and confining dose escalation to the target depends on excellent imaging.

Magnetic resonance imaging (MRI) has been widely used in combination with computed tomography (CT) for planning radiotherapy treatment, because its superior soft-tissue contrast can substantially improve segmentation accuracy in the brain, head-neck, prostate, and other regions [4]. In the diagnosis and management of liver tumors, Gadolinium-ethoxybenzyl-diethylenetriamine pentaacetic acid (Gd-EOB-DTPA)-enhanced MRI (i.e., EOB-MRI) has an important role, and it is widely used in clinical examinations [5–7] as well as in radiotherapy treatment planning [4,8–10].

The implantation of fiducial markers is recommended for precise CT-MRI registration in treatment planning, image localization in pretreatment patient-setup verification, and real-time tumor tracking during SBRT [11,12]. However, conventionally used gold fiducial markers are small in size (e.g., less than 1 mm in diameter) with low magnetic susceptibilities [13], which makes detection using MRI difficult. A previous study employed the T2*-weighted image for marker detection in

prostate radiotherapy because of its high metal sensitivity [14]. However, T2*-weighted images are inappropriate for tumor imaging in EOB-MRI, as there is a lack of tissue contrast between the tumor and normal liver parenchyma. Some previous studies have evaluated the characteristics of fiducial markers in MRI and provided guidance on the selection of suitable markers in clinical practice [13,15]; they concluded that obtaining multiple sequences was important for marker detection and tumor delineation. However, multiple scanning may cause misalignment and anatomical deformation, owing to different breath-holding positions in the liver. Thus, the application of a single imaging sequence capable of simultaneously detecting markers and delineating tumors would be ideal.

It is well known that the signal void induced by T2*-decay of metals depends on the echo time (TE), and that the bandwidth (BW) can affect magnetic susceptibility artifacts [13,16]. Therefore, we hypothesized that optimizing the parameters of the three-dimensional (3D) T1-weighted turbo gradient-echo sequence (T1W-GRE), which is commonly used in EOB-MRI, would enable identification of even small gold fiducial markers without compromising tumor delineation. Although some studies have demonstrated the sequence dependence of marker detection [13,14], to the best of our knowledge, this is the first study on the optimization of imaging parameters for marker detection in liver.

This study aimed to optimize the parameters of 3D T1W-GRE, focusing on both high metal sensitivity and sufficient tumor/normal-tissue T1 contrast, by using a custom-made phantom. We also

compared the image quality of the resulting sequence (named “HYBRID”) with that of a conventional one using clinical data.

Materials and Methods

All scans were performed on a 3T MRI scanner (MAGNETOM Skyra, Siemens Healthcare, Erlangen, Germany) using a combined 18-channel matrix body and spine coil. The volumetric interpolated breath-hold examination (VIBE) technique [17] was used as the base sequence for 3D T1W-GRE.

Phantom study

Custom-made phantom

For simulating tumor and normal liver parenchyma in the hepatobiliary phase, respectively, 0.1 and 0.2 mmol/L of gadoxetate sodium (EOB-Primovist, Bayer Yakuhin, Ltd., Osaka, Japan [Gd-EOB]) diluted with distilled water were prepared and gelled with 2% agar. The precontrast and postcontrast T1 values reported in [18] were respectively regarded as those of tumor and liver parenchyma in the hepatobiliary phase. The final T1 and T2 values of each solution (measured by inversion-recovery and single spin-echo methods, respectively) were 883 ms for T1 and 66 ms for T2 in the tumor-vial, 530 ms for T1 and 62 ms for T2 in the parenchyma-vial. In addition, a VISICOIL™ (>99.9% Au, SCETI Medical Labo KK, Tokyo, Japan) with diameter 0.5 mm and length 5 mm was embedded in the parenchyma-vial, and both vials were placed in a container. The surroundings were filled with rice to minimize the B0 inhomogeneity at the vial/air-interface (Fig. 1).

Acquisition and analysis

For determining the optimal parameters, phantom images were obtained with 3D-VIBE by varying TE, BW, flip angle (FA), and base matrix size. The basic parameters were TE, 2.5 ms; BW, 400 Hz/pixel; FA, 10°, and base matrix size, 256. TE was varied from 1.5 ms to 4.0 ms at 0.5 ms intervals. BW was varied to 200, 300, 400, 500, 610, and 700 Hz/pixel. FA was varied from 5° to 30° in 5° intervals. The base matrix size was varied from 256 to 416 in 32-step intervals. When one parameter is varied, all other parameters were fixed at the basic values described above. The other common parameters were set as follows: repetition time, 6.5 ms; field-of-view, 285 × 380 mm^2; slice thickness, 2 mm; number of slices, 60; parallel-imaging acceleration factor, 2 for the slice direction using the CAIPIRINHA technique [19], and number of averages, 1. The chemical shift selective pulse method was employed for fat-suppression.

For comparison at each parameter setting, the signal intensity (SI) and its standard deviation (SD) were measured; moreover, the region of interest (ROI) was defined manually. To measure the signal-to-noise ratio (SNR) and contrast ratio (CR), we first identified a slice that did not contain metal artifacts, and carefully set the ROI such that no air bubbles were contained therein. The SNR was calculated as $SNR = SI/SD,$ where SI is the mean value within the ROI, and SD is measured for an identical ROI in the parenchyma-vial. The CR was calculated as $CR = (SI\ of\ Parenchyma\text{-}vial - SI\ of\ Tumor\text{-}vial) / (SI\ of\ Parenchyma\text{-}vial + SI\ of\ Tumor\text{-}vial)$, where SI is the mean value within the ROI. The ROI in the parenchyma-vial was the same as that in the case of SNR measurement, and that

in the tumor-vial was drawn with the same size at the same slice. To evaluate marker detection, we selected the slice with the most prominent metal artifacts (i.e., different slice from SNR and CR measurements), and the relative standard deviation (RSD) was calculated as $RSD\ [\%] = (SD/SI) \times 100$. Here, we used the SD and mean values within the manually drawn ROI that were as large as possible to include the metal artifacts induced by the VISICOIL, and to exclude the edge of the parenchyma-vial. Within a homogeneous phantom, the clarity of the signal void and the presence of susceptibility artifacts can affect the RSD. Thus, a larger RSD implies better marker visibility. Ten scans were performed for each parameter setting, and the average value was used (10 sets of data each).

The HYBRID sequence was determined from the results of preliminary experiments, considering the total balance of the large RSD for better marker detection, and sufficient SNR and CR values for tumor delineation, with a suitable breath-holding acquisition time (limited to 23 s). Subsequently, the sequence was quantitatively evaluated by comparison with the conventional 3D-VIBE sequence (C-VIBE) and two-dimensional T2*-weighted gradient-echo sequence (T2*) in terms of the SNR, CR, and RSD. We performed the ROI placement similar to the one in the preliminary experiment but selected three slices for this case. Because marker-visibility is also affected by expansion artifacts into the though-plane in the RSD measurement, the ROI placement was performed in three slices where metal artifacts were visible. For the SNR and CR measurements, the ROI placement was performed in three slices without metal artifacts. Ten scans were performed for each

parameter setting, and the average value was used (30 sets of data each). The detailed parameters for all three sequences are listed in Table 1.

Clinical study

The study was approved by the ethics committee of our institution. Informed consent was waived by the committee, because clinical MRI data were collected retrospectively.

Subjects

Data were collected from six patients (mean age, 73.2 years; range, 66–82 years) who underwent EOB-MRI for radiotherapy from January 2021 to June 2021 at Nagoya University Hospital. Five patients were being treated for hepatocellular carcinoma and one for intrahepatic cholangiocarcinoma. All patients received ultrasound-guided marker implantation as part of our standard clinical practice. The VISICOIL ™ (>99.9% Au, Φ 0.5 mm, length: 5 mm) used in our institution contains a pair of markers; hence, a total of two markers should be visualized. A dynamic contrast-enhanced CT scan was performed one week after marker implantation, and EOB-MRI was performed the day after the CT scan.

Acquisition and analysis

All patients were scanned with C-VIBE and the newly determined HYBRID. Both sequences were acquired 15–20min after administration of Gd-EOB, i.e., in the hepatobiliary phase. For comparison and reliable marker detection, T2* was acquired approximately 5 min after administration. The same scan parameters used for the phantom study were used in the clinical examination. The vendor-

provided 3D distortion correction was applied to ensure the geometric accuracy [20], and geometric distortion was minimized by positioning tumor and markers as close as possible to the center of the Z-axis of the MRI bed.

For qualitative assessment, a radiation oncologist and a medical physicist with six and eight years of experience in radiotherapy, respectively, were blinded to the acquisition techniques, and performed independent visual assessments. They ranked marker detection, tumor delineation, and overall image quality, using a four-point scale. For marker detection, the scale was as follows: 1 = non-identifiable; 2 = obscured even with CT-combination; 3 = identifiable with CT-combination; and 4 = clearly identifiable. Here, "CT-combination" means that the CT image was used to locate the marker and was scored with the corresponding MRI individually. It should be noted that there were two markers for each patient, and these were evaluated individually. For tumor delineation, the scale was as follows: 1 = non-identifiable; 2 = obscured or blurred with some effect on contouring quality; 3 = almost clear with no effect on contouring quality; and 4 = clearly identifiable. For overall image quality, the scale was as follows: 1 = poor; 2 = suboptimal; 3 = acceptable; and 4 = excellent.

Statistical analysis

All statistical analyses were performed using the SPSS software (SPSS for Windows, version 27, IBM). The Friedman test with Bonferroni correction was employed to test the differences in SNR, CR, and RSD for the three sequences in the phantom study. The Wilcoxon signed-rank test was employed to compare the two sequences (C-VIBE and HYBRID) for marker detection, tumor

delineation, and overall image quality in the clinical study. A P-value of < 0.05 was considered statistically significant.

Results

Phantom study

Figure 2 shows the changes in SNR, CR, and RSD caused by varying TE, BW, FA, and base matrix size. SNR showed no obvious dependence on TE, but decreased with a higher BW and larger base matrix size. The maximum SNR value was obtained at 10° when the FA was varied. CR increased with a larger FA but was not affected by any other parameters. On the contrary, RSD was highly dependent on TE. It also decreased slightly for a larger FA and increased with a larger base matrix size, but it was independent of BW. The boxplots in Fig. 3 compare the three sequences for the SNR, CR, and RSD. HYBRID showed significantly higher SNR and RSD values than those of C-VIBE ($P <$ 0.001); the RSD in this case was significantly different from that of T2* ($P = 0.029$). Although the CRs of HYBRID and C-VIBE were statistically different ($P = 0.014$), they were extremely close, whereas the CR of T2* was considerably lower.

Clinical study

Table 2 presents the scores for marker detection, tumor delineation, and overall image quality of the three sequences. In marker detection, HYBRID outscored C-VIBE (mean score: 3.5 ± 0.8 vs. $2.2 \pm$ 0.9, $P < 0.001$), whereas the tumor delineation and overall image quality scores of the two sequences

were not significantly different statistically (3.6 ± 0.5 vs. 3.7 ± 0.5, $P = 0.56$ and 3.6 ± 0.5 vs. 3.8 ± 0.5, $P = 0.32$, respectively). T2* had the highest score in marker detection, but its tumor delineation and overall image quality scores were markedly inferior, although no statistical analysis was performed. Representative images corresponding to Case 1 are shown in Fig. 4 (see Supplementary data for all other cases).

Discussion

The visualization of fiducial markers is important for precise CT-MRI registration in liver SBRT; simultaneous marker detection and tumor delineation in a single sequence would be ideal for avoiding misalignment due to separate breath-holding positions in multiple imaging rounds. Therefore, we first used phantom experiments to determine the parameters of the modified sequence, focusing on both high metal sensitivity and sufficient tumor/normal-tissue T1 contrast. We also performed visual assessments using clinical images. Our results demonstrated that the newly optimized sequence allowed for better gold fiducial marker detection without degrading tumor delineation in the primary liver tumor.

The effect of metals on MRI is represented as signal voids or pile-ups due to decreased local-T2* and susceptibility artifacts caused by B0 inhomogeneity. In EOB-MRI, 3D T1W-GRE is the indispensable sequence for obtaining the Gd-EOB enhancement effect. However, T1-weighted sequences are inferior to T2*-weighted sequences for marker detection in the prostate, as

demonstrated previously [14]. Small markers are also difficult to detect on MRI, and are sometimes invisible even with T2*-weighted images [21]. To overcome this constraint, iron-containing (i.e., ferromagnetic) [22] or platinum (i.e., paramagnetic) [23] markers have been developed, which have a higher magnetic susceptibility than that of gold (i.e., diamagnetic), and can produce larger artifacts that are easier to detect. However, these markers are disadvantageous because local distortions caused by the implantation of these markers (iron-containing or platinum) can potentially compromise the geometric accuracy. Recently, a novel liquid marker (BioX-mark) without metals has been reported, which causes the formation of signal voids due to the lack of water protons. This would be ideal in terms of local susceptibility distortion [24]. Although using such markers may be a feasible solution, many hospitals still use gold markers. Therefore, in this study, we addressed the detection of gold fiducial markers using parameter optimization.

In the phantom study, the RSD was used as an indicator of marker detection, and a longer TE resulted in a larger RSD (Fig. 2-i) due to an enhancement of the signal void. Although a previous study evaluated the characteristics of various markers by separating signal void and susceptibility artifacts [13], we employed the RSD to evaluate these two factors in combination. Our study focused on the determination of parameters for clinical use, and RSD was sufficient for this purpose. The result was also consistent with that of clinical visual assessment. In contrast, BW showed little impact on RSD in our study (Fig. 2-j), whereas a previous study found that markers were significantly less pronounced in higher-BW images [16]. This discrepancy may be because of the differences in BW,

marker size, and spatial resolution. They used relatively low BWs and high spatial resolution to understand the principles of marker detection, whereas, we conducted our evaluation under conditions designed for clinical situations.

Another finding was that higher in-plane resolution was preferable for marker detection (Fig. 2-l) because of the clear visualization of signal void. Therefore, we employed a large TE (modified to 3.5 ms from 1.78 ms) and base matrix size (modified to 320 from 256) to improve marker detection, with the trade-off of longer acquisition time and decreased SNR. The extension of TR due to long TE and increased matrix size results in longer acquisition time. To address the lengthening of the acquisition time, we reduced the number of slices and applied the phase-partial-Fourier technique (see Table 1). SNR theoretically decreases with increasing matrix size and reducing the number of slices, nevertheless, the SNR of HYBRID was higher than that of C-VIBE. One possible explanation is that the unintentionally longer TR due to TE extension caused a signal increase. In addition, we set the BW such that it was smaller than C-VIBE to increase the SNR (modified to 400 Hz/pixel from 470 Hz/pixel). Thus, the increase in SNR obtained due to long TR and lower BW outweighed its decrease due to the large matrix size and reduced number of slices. Thus, HYBRID had an acceptable acquisition time, considerably improved gold marker detection, and comparable tissue T1-contrast relative to a conventional sequence.

In the clinical study, C-VIBE failed to identify the markers in most cases. In contrast, HYBRID was able to identify all markers except one. The marker in Case 3 could not be identified

(see Supplementary Fig.2), because it was located at the edge of the liver parenchyma and was not clearly discernible even with T2*. In other cases, the scores for marker detection were either 3 or 4 (identifiable), and tumor delineation and overall image quality were acceptable. Particularly in case 2, the markers had been implanted at the radiofrequency ablation site, not the liver parenchyma (i.e., the background signal was relatively low); nevertheless, they were clearly identifiable on the HYBRID image because of enhanced signal void (see Supplementary Fig. 1). T2* had the highest score in marker detection in most cases (as expected). However, its scores in tumor delineation and overall image quality were extremely low, suggesting that it is inappropriate for tumor contouring in liver.

HYBRID allowed for small non-iron markers to be visualized without degrading the tumor/normal-tissue contrast by Gd-EOB, which would lead to more accurate and efficient treatment planning. Our parameter optimization did not involve any new technology prior to commercialization and is easily reproducible on normal clinical scanners. HYBRID can also reduce the burden on the patient by reducing the number of breath-holds during examination, because multiple sequences are not required. However, slight lip-like artifacts were observed in some cases (an example is shown in the form of dotted arrows in Fig. 4), which may have been caused by imperfect breath-holding due to the longer acquisition time (e.g., the score of observer A for the overall image quality in cases 3 and 5 was also 3, due to this artifact, which is not shown here). Further optimization to reduce the time would be desirable in the future, especially for patients with difficulties in breath-holding.

When using multiple sequences for marker detection and tumor delineation, both the difference in breath-hold level and the deformation of the abdominal anatomy affects the registration. There is a respiratory-induced anatomical deformation of the liver itself, and the deformation of the abdominal anatomy during each of the respiratory phases also affects the liver shape. To understand the tumor deformation during each of the respiratory phases (e.g., inspiration and expiration), it is necessary to visualize the marker and tumor simultaneously. The proposed sequence may be useful for this aspect as well.

Our study involved only primary liver tumors, which are a minority of patients targeted for SBRT. A majority of targets for SBRT are metastatic liver tumors, but we could not include metastatic tumors because they are treated with other treatment options in our hospital. Therefore, the number of cases is very limited and the proposed sequence has not been confirmed to be useful for metastatic tumors as well. However, both the primary and metastatic liver tumors show the same low signal in the hepatobiliary phase of EOB-MRI because of the lack of normal hepatocytes. In addition, because metastatic tumor is not associated with liver dysfunction, there would be a greater uptake of Gd-EOB into the normal liver parenchyma [25,26], which would provide a better contrast between the background liver (high signal) and the tumor or marker (low signal). HYBRID has the potential to be widely used for liver SBRT, including metastatic tumors, although it needs to be confirmed in metastatic cases in the future.

There are some limitations to this study. First, the number of subjects was small, and only

primary liver tumors were included. Future studies should be conducted to explore the cases of metastatic liver tumors. Second, the marker characteristics were not considered and only one type of marker was used. Several previous studies have indicated that marker visibility depends on size, shape, composition, and orientation [13,15,21]. However, we focused on determining the parameter settings, and understanding the effects of marker characteristics was beyond the scope of the present study. Smaller markers can mitigate the invasiveness of marker implantation and produce fewer CT artifacts; therefore, a future study needs to confirm whether a marker of diameter 0.35 mm (the smallest non-iron fiducial marker commercially available) can be visualized. Third, our study was performed with a 3T scanner. High magnetic fields generally have a high metal sensitivity [15] and better contrast enhancement caused by the prolongation of T1 relaxation times [27]. Hence, further parameter optimization may be necessary when using 1.5 T scanners.

Conclusions

The proposed HYBRID sequence can improve gold fiducial marker detection without degrading tumor delineation in EOB-MRI for SBRT of primary liver tumor. It suggests that parameter optimization is important for marker detection on MRI. Our findings may lead to more accurate and efficient treatment planning, and also reduce the burden on patients by reducing the number of breath-holds during examination. Future studies in patients with metastatic liver tumors are required for a widespread use.

Declaration of Competing Interest

The authors declare that they have no known competing financial interests or personal relationships that could have appeared to influence the work reported in this paper.

Funding

This research did not receive any specific grant from funding agencies in the public, commercial, or not-for-profit sectors.

References

[1] Liu E, Stenmark MH, Schipper MJ, Balter JM, Kessler ML, Caoili EM, et al. Stereotactic body radiation therapy for primary and metastatic liver tumors. Transl Oncol 2013;6:442–6. https://doi.org/10.1593/tlo.12448.

[2] Méndez Romero A, de Man RA. Stereotactic body radiation therapy for primary and metastatic liver tumors: From technological evolution to improved patient care. Best Pract Res Clin Gastroenterol 2016;30:603–16. https://doi.org/10.1016/j.bpg.2016.06.003.

[3] Doi H, Beppu N, Kitajima K, Kuribayashi K. Stereotactic body radiation therapy for liver tumors: Current status and perspectives. Anticancer Res 2018;38:591–9. https://doi.org/10.21873/anticanres.12263.

[4] Schmidt MA, Payne GS. Radiotherapy planning using MRI. Phys Med Biol 2015;60:R323–61. https://doi.org/10.1088/0031-9155/60/22/R323.

[5] Kudo M. Will Gd-EOB-MRI change the diagnostic algorithm in hepatocellular carcinoma? Oncology 2010;78:87–93. https://doi.org/10.1159/000315235.

[6] Ichikawa T, Sano K, Morisaka H. Diagnosis of pathologically early HCC with EOB-MRI: Experiences and current consensus. Liver Cancer 2014;3:97–107. https://doi.org/10.1159/000343865.

[7] Tamada T, Ito K, Sone T, Kanki A, Sato T, Higashi H. Gd-EOB-DTPA enhanced MR imaging: Evaluation of biliary and renal excretion in normal and cirrhotic livers. Eur J Radiol 2011;80:e207–11. https://doi.org/10.1016/j.ejrad.2010.08.033.

[8] Rosenberg SA, Henke LE, Shaverdian N, Mittauer K, Wojcieszynski AP, Hullett CR, et al. A Multi-Institutional Experience of MR-Guided Liver Stereotactic Body Radiation Therapy. Adv Radiat Oncol 2019;4:142–9. https://doi.org/10.1016/j.adro.2018.08.005.

[9] Tsegmed U, Kimura T, Nakashima T, Nakamura Y, Higaki T, Imano N, et al. Functional image-guided stereotactic body radiation therapy planning for patients with hepatocellular carcinoma. Med Dosim 2017;42:97–103. https://doi.org/10.1016/j.meddos.2017.01.005.

[10] Wojcieszynski AP, Rosenberg SA, Brower J V., Hullett CR, Geurts MW, Labby ZE, et al. Gadoxetate for direct tumor therapy and tracking with real-time MRI-guided stereotactic body radiation therapy of the liver. Radiother Oncol 2016;118:416–8. https://doi.org/10.1016/j.radonc.2015.10.024.

[11] Scher N, Bollet M, Bouilhol G, Tannouri R, Khemiri I, Vouillaume A, et al. Safety and efficacy of fiducial marker implantation for robotic stereotactic body radiation therapy with fiducial tracking. Radiat Oncol 2019;14:167. https://doi.org/10.1186/s13014-019-1373-2.

[12] Park SH, Won HJ, Kim SY, Shin YM, Kim PN, Yoon SM, et al. Efficacy and safety of ultrasound-guided implantation of fiducial markers in the liver for stereotactic body radiation therapy. PLoS One 2017;12:0–3. https://doi.org/10.1371/journal.pone.0179676.

[13] Gurney-Champion OJ, Lens E, Van Der Horst A, Houweling AC, Klaassen R, Van Hooft JE,

et al. Visibility and artifacts of gold fiducial markers used for image guided radiation therapy of pancreatic cancer on MRI. Med Phys 2015;42:2638–47. https://doi.org/10.1118/1.4918753.

[14] Tanaka O, Komeda H, Hattori M, Hirose S, Yama E, Matsuo M. Comparison of MRI sequences in ideal fiducial maker-based radiotherapy for prostate cancer. Reports Pract Oncol Radiother 2017;22:502–6. https://doi.org/10.1016/j.rpor.2017.10.002.

[15] Chan MF, Cohen GN, Deasy JO. Qualitative Evaluation of Fiducial Markers for Radiotherapy Imaging. Technol Cancer Res Treat 2015;14:298–304. https://doi.org/10.1177/1533034614547447.

[16] Jonsson JH, Garpebring A, Karlsson MG, Nyholm T. Internal fiducial markers and susceptibility effects in MRI - Simulation and measurement of spatial accuracy. Int J Radiat Oncol Biol Phys 2012;82:1612–8. https://doi.org/10.1016/j.ijrobp.2011.01.046.

[17] Rofsky NM, Lee VS, Laub G, Pollack MA, Krinsky GA, Thomasson D, et al. Abdominal MR imaging with a volumetric interpolated breath-hold examination. Radiology 1999;212:876–84. https://doi.org/10.1148/radiology.212.3.r99se34876.

[18] Katsube T, Okada M, Kumano S, Hori M, Imaoka I, Ishii K, et al. Estimation of liver function using T1 mapping on Gd-EOB-DTPA-enhanced magnetic resonance imaging. Invest Radiol 2011;46:277–83. https://doi.org/10.1097/RLI.0b013e318200f67d.

[19] Yu MH, Lee JM, Yoon JH, Kiefer B, Han JK, Choi BI. Clinical application of controlled aliasing in parallel imaging results in a higher acceleration (CAIPIRINHA)-volumetric interpolated breathhold (VIBE) sequence for gadoxetic acid-enhanced liver MR imaging. J Magn Reson Imaging 2013;38:1020–6. https://doi.org/10.1002/jmri.24088.

[20] Karger CP, Höss A, Bendl R, Canda V, Schad L. Accuracy of device-specific 2D and 3D image distortion correction algorithms for magnetic resonance imaging of the head provided by a manufacturer. Phys Med Biol 2006;51. https://doi.org/10.1088/0031-9155/51/12/N04.

[21] Tanaka O, Komeda H, Tamaki M, Seike K, Fujimoto S, Yama E, et al. Comparison of MRI visualization between linearly placed iron-containing and non-iron-containing fducial markers for prostate radiotherapy. Br J Radiol 2018;91:1–4. https://doi.org/10.1259/bjr.20170612.

[22] Tanaka O, Nishigaki Y, Hayashi H, Iida T, Yokoyama T, Takenaka E, et al. The advantage of iron-containing fiducial markers placed with a thin needle for radiotherapy of liver cancer in terms of visualization on MRI: an initial experience of Gold Anchor. Radiol Case Reports 2017;12:416–21. https://doi.org/10.1016/j.radcr.2017.03.014.

[23] Singhrao K, Ruan D, Fu J, Gao Y, Chee G, Yang Y, et al. Quantification of fiducial marker visibility for MRI-only prostate radiotherapy simulation. Phys Med Biol 2020;65. https://doi.org/10.1088/1361-6560/ab65db.

[24] Schneider S, Jølck RI, Troost EGC, Hoffmann AL. Quantification of MRI visibility and artifacts at 3T of liquid fiducial marker in a pancreas tissue-mimicking phantom. Med Phys 2018;45:37–47. https://doi.org/10.1002/mp.12670.

[25] Velec M, Moseley JL, Craig T, Dawson LA, Brock KK. Accumulated dose in liver stereotactic

body radiotherapy: Positioning, breathing, and deformation effects. Int J Radiat Oncol Biol Phys 2012;83:1132–40. https://doi.org/10.1016/j.ijrobp.2011.09.045.

[26] Von Siebenthal M, Sźkely G, Lomax AJ, Cattin PC. Systematic errors in respiratory gating due to intrafraction deformations of the liver. Med Phys 2007;34:3620–9. https://doi.org/10.1118/1.2767053.

[27] Morita K, Namimoto T, Awai K, Komi M, Hashida M, Tsuji T, et al. Enhancement effects of hepatic dynamic MR imaging at 3.0 T and 1.5 T using gadoxetic acid in a phantom study: Comparison with gadopentetate dimeglumine. Magn Reson Med 2011;66:213–8. https://doi.org/10.1002/mrm.22770.

Figure captions

Fig. 1. (a) Photograph of VISICOIL™ (>99.9% Au) employed as a gold fiducial marker in this study. (b) Custom-made phantom. (c) Schematic of the two vials comprising the phantom, and location of the VISICOIL. For simulating tumor (left) and normal liver parenchyma (right), 0.1 and 0.2 mmol/L of gadoxetate sodium were diluted with distilled water and gelled with 2% agar, respectively. A VISICOIL was embedded in the right vial.

Fig. 2. Changes in (a – d) signal-to-noise ratio (SNR), (e – h) contrast ratio (CR), and (i – l) relative standard deviation (RSD) of the signal intensity with echo time, bandwidth, flip angle, and base matrix size.

Fig. 3. Boxplots comparing signal-to-noise ratio (SNR), contrast ratio (CR), and relative standard deviation (RSD) of the signal intensity for the three sequences; conventional (C-VIBE), HYBRID (this work), and T2*. Asterisks in plots indicate $P < 0.001$.

Fig. 4. Case 1 of a 66-year-old man with hepatocellular carcinoma with Child-Pugh A cirrhosis: (a) Post-contrast CT shows clear marker visibility. (b) Low-signal feature in T2*-weighted image shows the marker, but other similar low-signal regions are due to fibrosis; tumor delineation is poor. (c) Moderately low-signal area in conventional T1-weighted image at the hepatobiliary phase delineates tumor excellently, but the marker is also moderately low signal and difficult to distinguish from vessels. (d) HYBRID image at the hepatobiliary phase exhibits both clear marker detection and tumor delineation, but there are slight lip-like artifacts (dotted arrows). Arrow: marker; Arrowhead: tumor.

Table 1. The detailed imaging parameters for all three sequences.

	C-VIBE	**HYBRID**	**T2***
Type	3D T1W-GRE	3D T1W-GRE	2D GRE
Repetition time (ms)	3.9	5.45	332
Echo time (ms)	1.78	3.5	6.0
Flip angle (°)	9	10	30
Field-of-view (mm)	285 × 380	285 × 380	285 × 380
Matrix size (phase × read)	154 × 256	180 × 320	130 × 288
Acquisition resolution (mm)	1.86 × 1.48 × 2.0	1.58 × 1.19 × 2.0	2.20 × 1.32 × 2.0
Reconstruction resolution (mm)	1.48 × 1.48 × 3.0	1.19 × 1.19 × 3.0	1.32 × 1.32 × 2.0
Bandwidth (Hz/Pixel)	470	400	430
Number of slices	72	60	30
Number of averages	1	1	1
Phase-partial Fourier	Off	7/8	7/8
Slice-partial Fourier	7/8	7/8	n.a.
Parallel imaging	CAIPIRINHA of 2	CAIPIRINHA of 2	GRAPPA of 2
Fat suppression	CHESS	CHESS	No
Acquisition time (s)	19	23	23

C-VIBE, conventional volumetric interpolated breath-hold examination; 3D, three-dimensional; T1W-GRE, T1-weighted turbo gradient-echo; 2D, two-dimensional; n.a., not applicable; CAIPIRINHA, controlled aliasing in parallel imaging results in higher acceleration; GPAPPA, generalized autocalibrating partially parallel acquisitions; CHESS, chemical shift selective

Table 2. The scores for marker detection, tumor delineation, and overall image quality of the three sequences.

		Marker detection						Tumor delineation			Overall image quality		
		C-VIBE		HYBRID		T2*		C-VIBE	HYBRID	T2*	C-VIBE	HYBRID	T2*
Mean ± SD		2.2 ± 0.9		3.5 ± 0.8		3.8 ± 0.5		3.7 ± 0.5	3.6 ± 0.5	1.7 ± 0.7	3.8 ± 0.5	3.6 ± 0.5	2.3 ± 0.7
Case 1	Observer A	2	1	4	3	4	2	4	3	1	4	3	2
	Observer B	3	2	4	4	4	3	4	4	2	3	3	3
Case 2	Observer A	1	1	4	4	4	4	4	4	1	4	4	1
	Observer B	2	2	4	3	4	4	3	3	1	4	4	2
Case 3	Observer A	2	1	4	1	4	3	3	3	3	4	3	3
	Observer B	2	1	3	2	4	3	3	3	2	4	4	2
Case 4	Observer A	3	1	4	3	4	4	4	4	1	4	4	2
	Observer B	4	2	4	4	4	4	3	4	2	3	4	2
Case 5	Observer A	3	2	4	3	4	4	4	4	1	3	3	3
	Observer B	3	2	4	4	4	4	4	3	2	4	3	3
Case 6	Observer A	3	3	4	4	4	4	4	4	2	4	4	2
	Observer B	3	3	3	3	4	4	4	4	2	4	4	3

Note that there were two markers for each patient, and these were evaluated individually. C-VIBE, conventional volumetric interpolated breath-hold examination; SD, standard deviation.

Fig. 1

(a) (b) (c)

Fig. 2

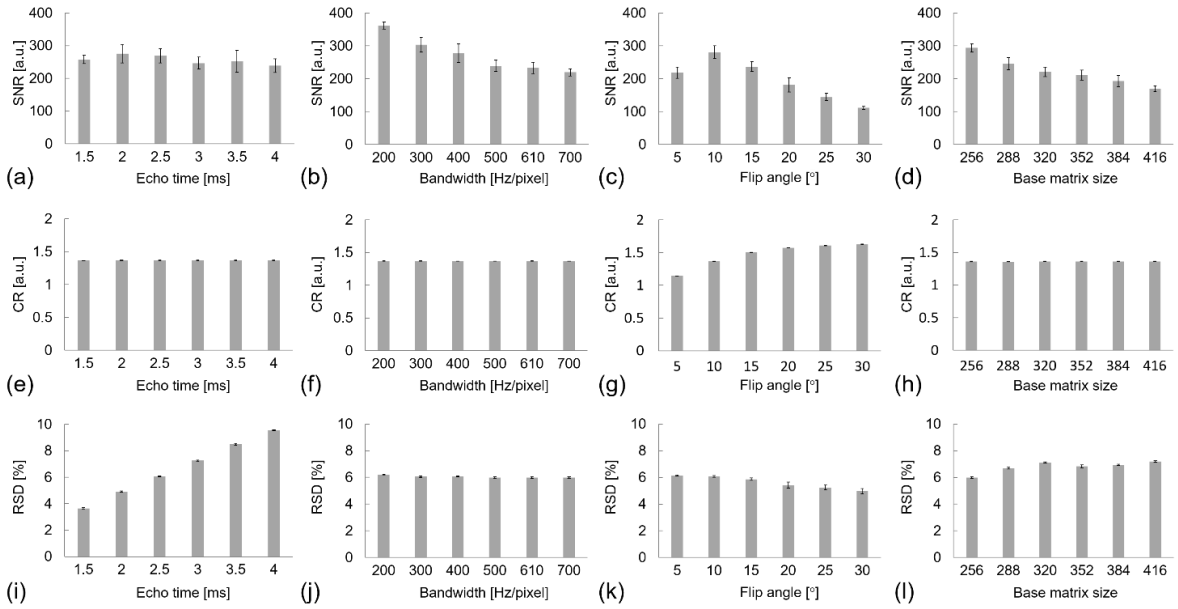
SNR [a.u.]
Echo time [ms]
(a)
Bandwidth [Hz/pixel]
(b)
Flip angle [°]
(c)
Base matrix size
(d)
CR [a.u.]
(e)
(f)
(g)
(h)
RSD [%]
(i)
(j)
(k)
(l)

Fig. 3

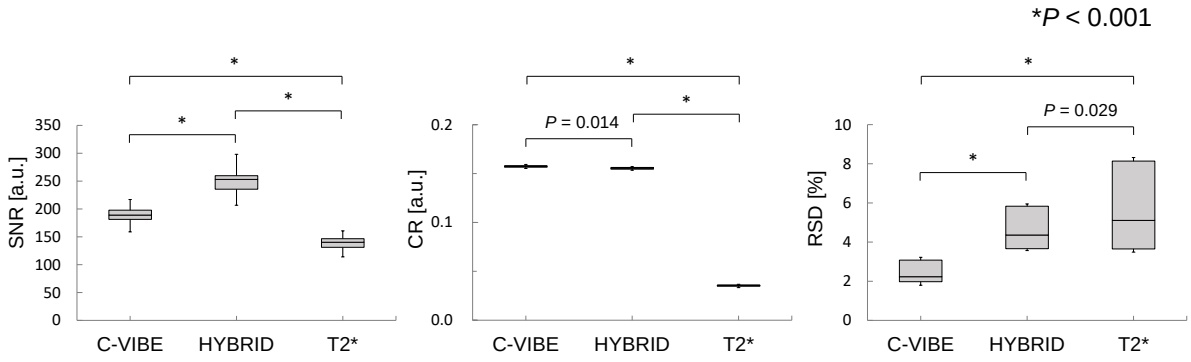

Fig. 4

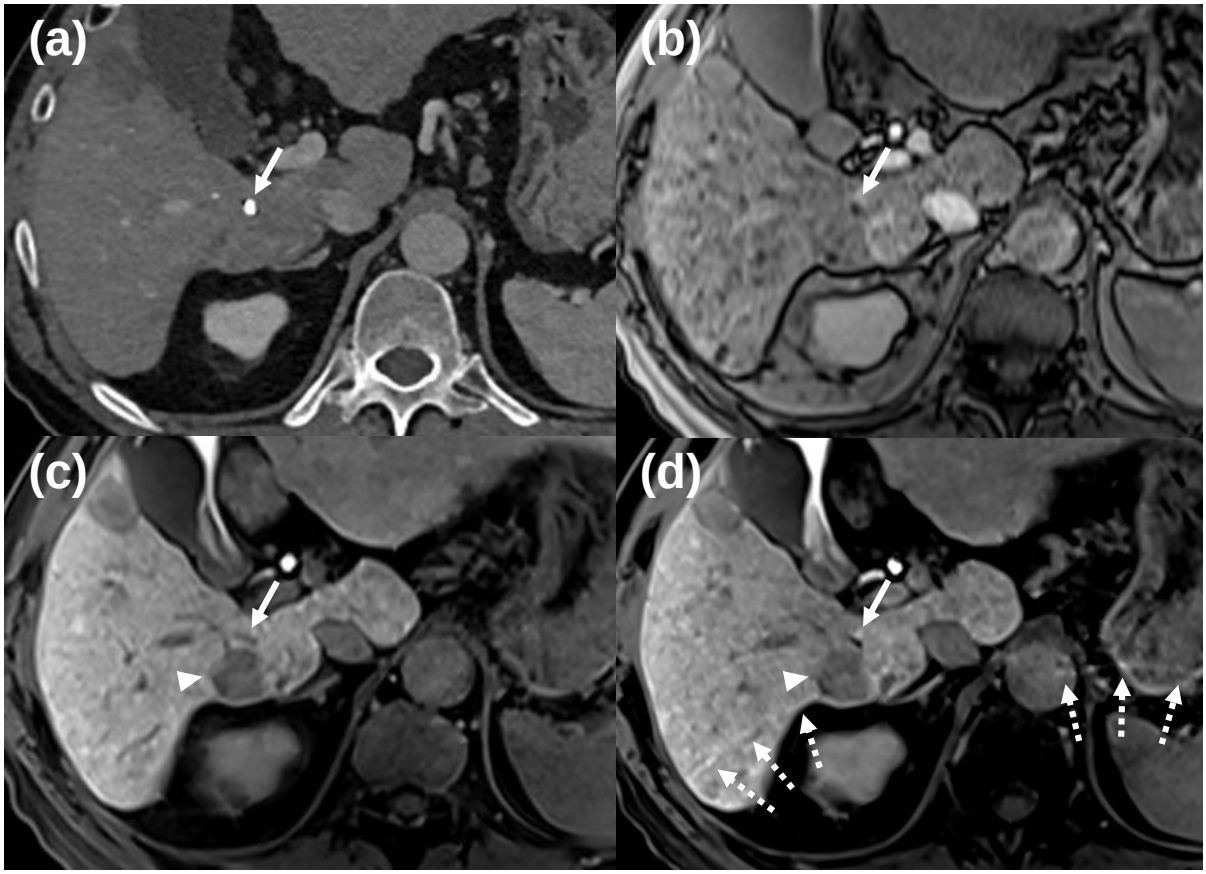

Appendix A. Supplementary data

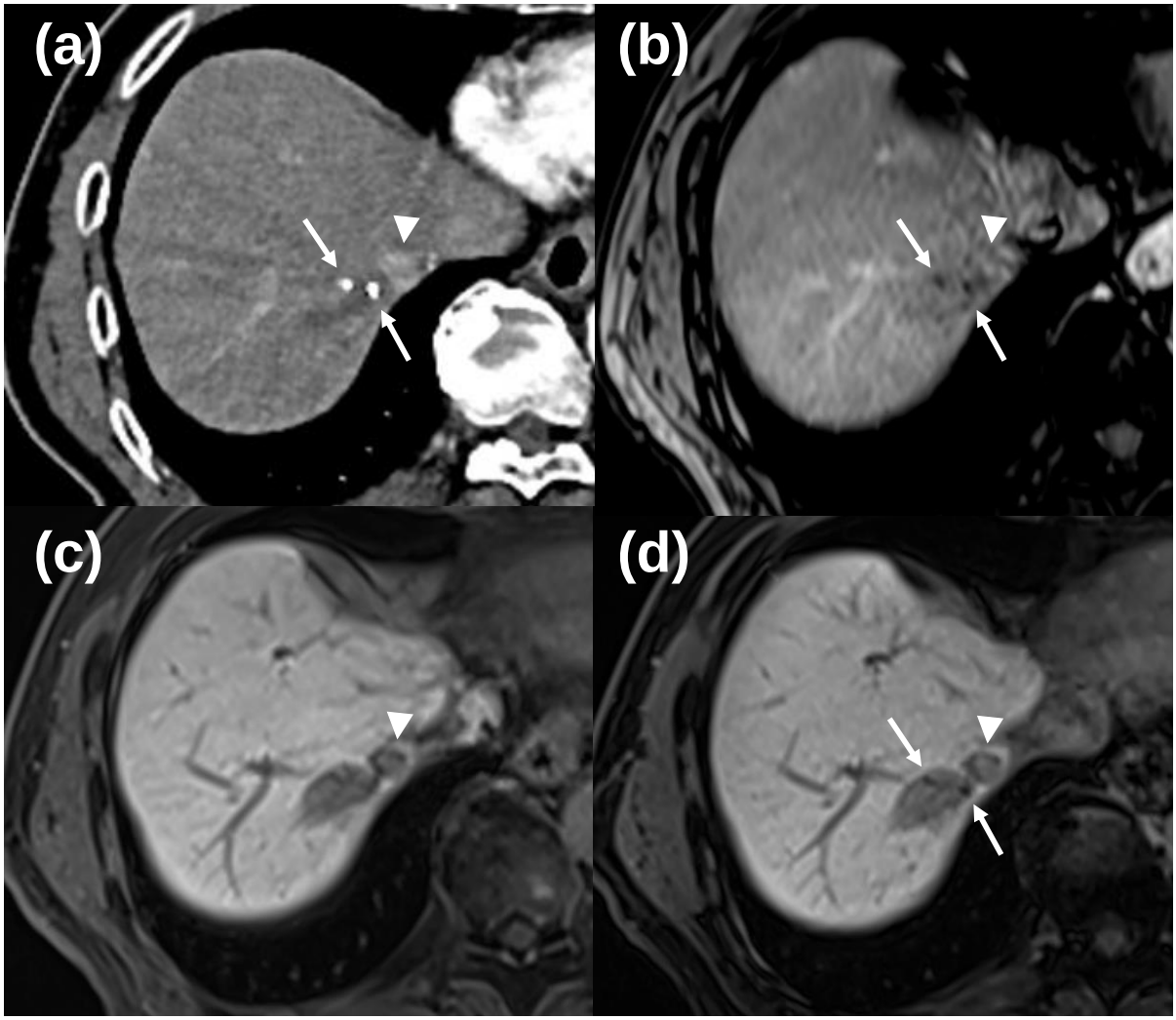

Supplementary Fig. 1. Case 2 of a 76-year-old man with hepatocellular carcinoma in hepatitis B virus with Child-Pugh A: (a) Post-contrast CT shows clear marker visibility. (b) T2*-weighted image shows sufficient marker detection, but the tumor is not distinguishable. (c) Conventional T1-weighted image at the hepatobiliary phase shows excellent tumor delineation, but the markers are not identifiable. (d) HYBRID image at the hepatobiliary phase shows marker detection even though the markers are in radiofrequency ablation site. Arrow: marker; Arrowhead: tumor.

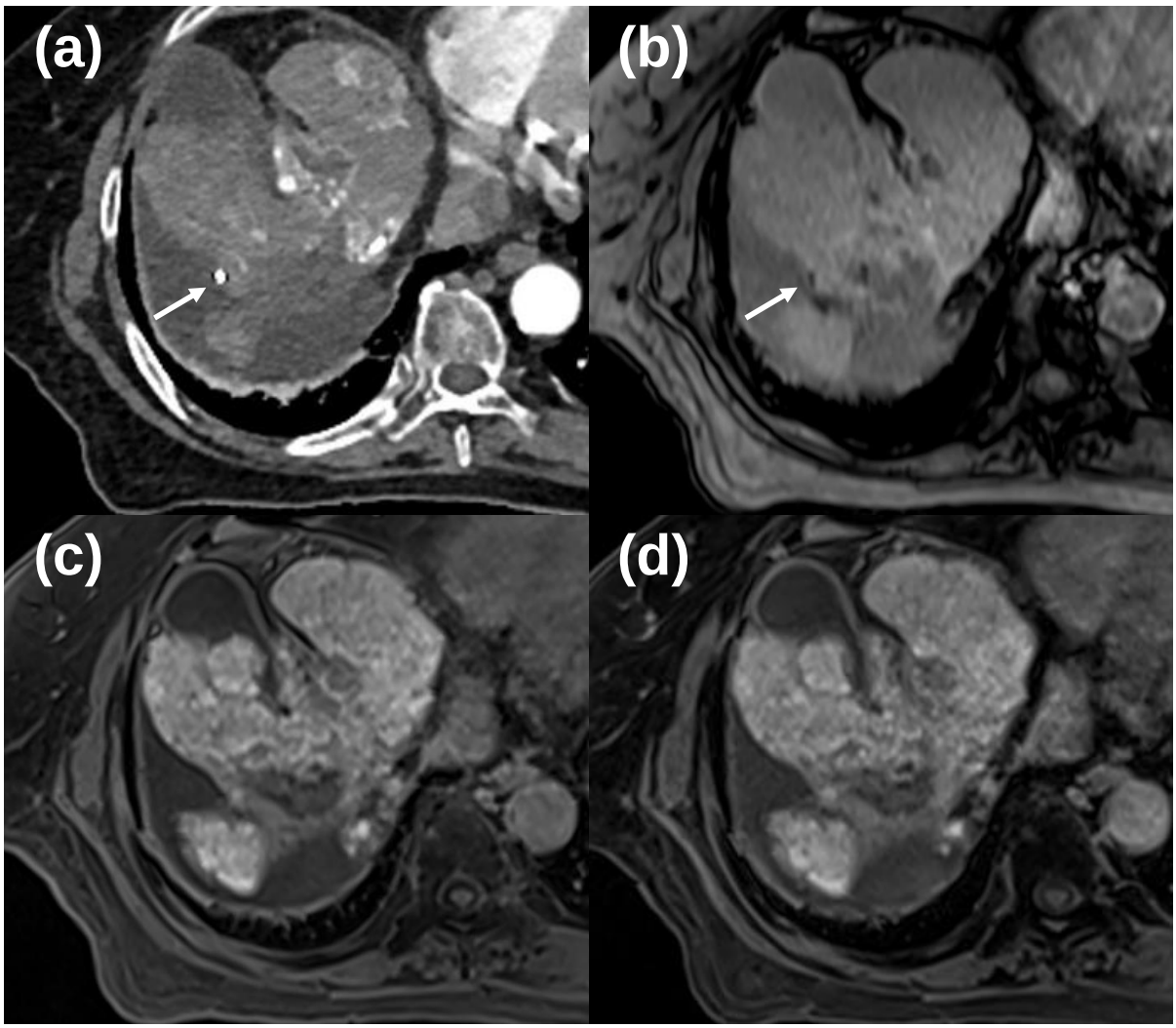

Supplementary Fig. 2. Case 3 of a 70-year-old woman with hepatocellular carcinoma with Child-Pugh A cirrhosis: (a) Post-contrast CT shows clear marker visibility. (b) T2*-weighted image shows the marker, even though it is at the edge of the liver parenchyma. (c – d) The marker is not detected in either conventional T1-weighted or HYBRID images at the hepatobiliary phase. Arrow: marker.

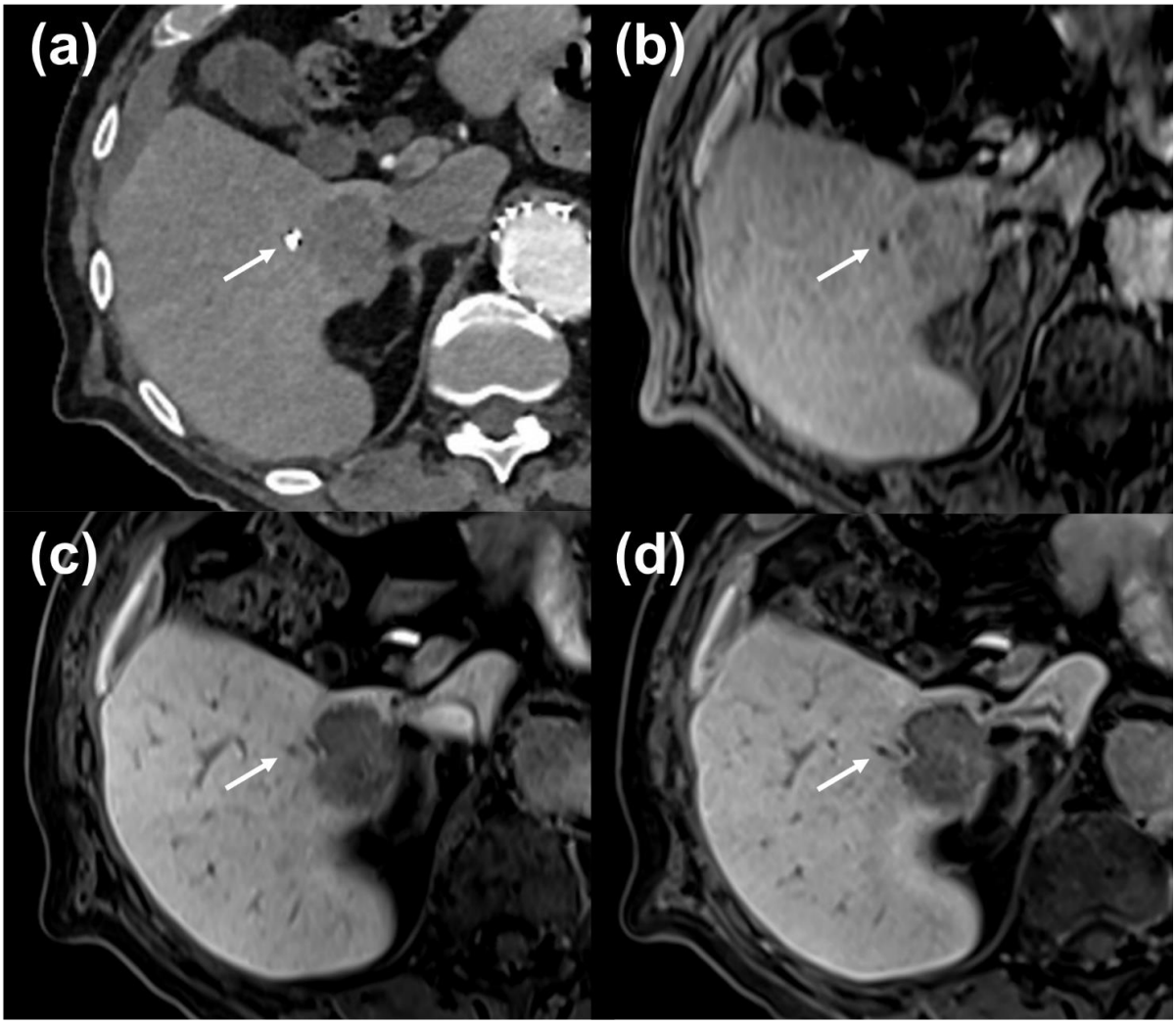

Supplementary Fig. 3. Case 4 of an 82-year-old man with intrahepatic cholangiocarcinoma: (a) Post-contrast CT shows clear marker visibility. (b) T2*-weighted image shows sufficient marker detection, but the tumor edges are obscured. (c) Conventional T1-weighted image at the hepatobiliary phase shows excellent tumor delineation, but the marker is unclear. (d) HYBRID image at the hepatobiliary phase exhibits both clear marker detection and tumor delineation. Arrow: marker.

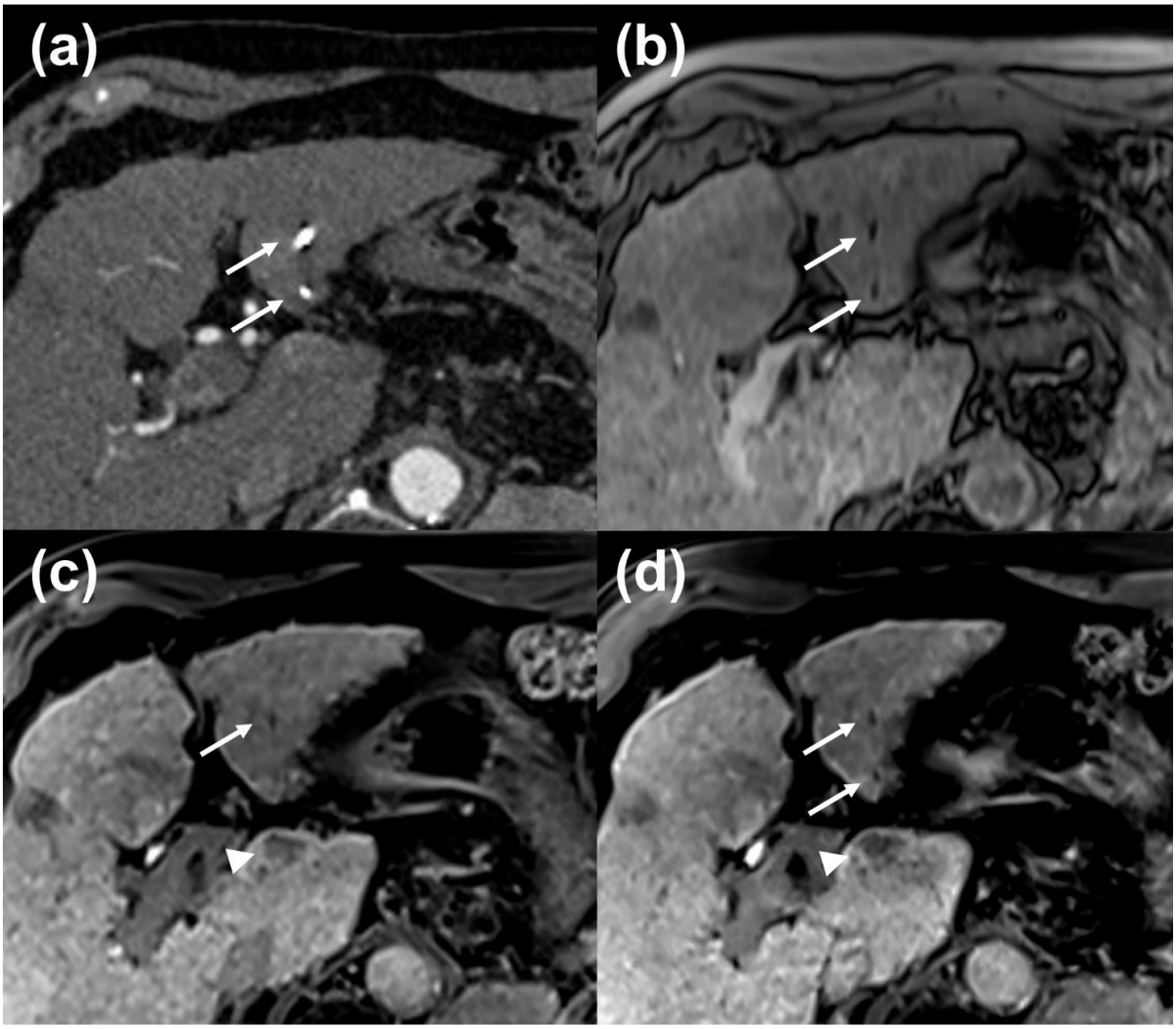

Supplementary Fig. 4. Case 5 of a 73-year-old man with hepatocellular carcinoma with Child-Pugh A cirrhosis: (a) Post-contrast CT shows clear marker visibility. (b) T2*-weighted image shows sufficient marker detection, but the tumor cannot be distinguished. (c) Conventional T1-weighted image at the hepatobiliary phase can identify one marker, but not the other. (d) HYBRID image at the hepatobiliary phase can identify both markers. Arrow: marker; Arrowhead: tumor.

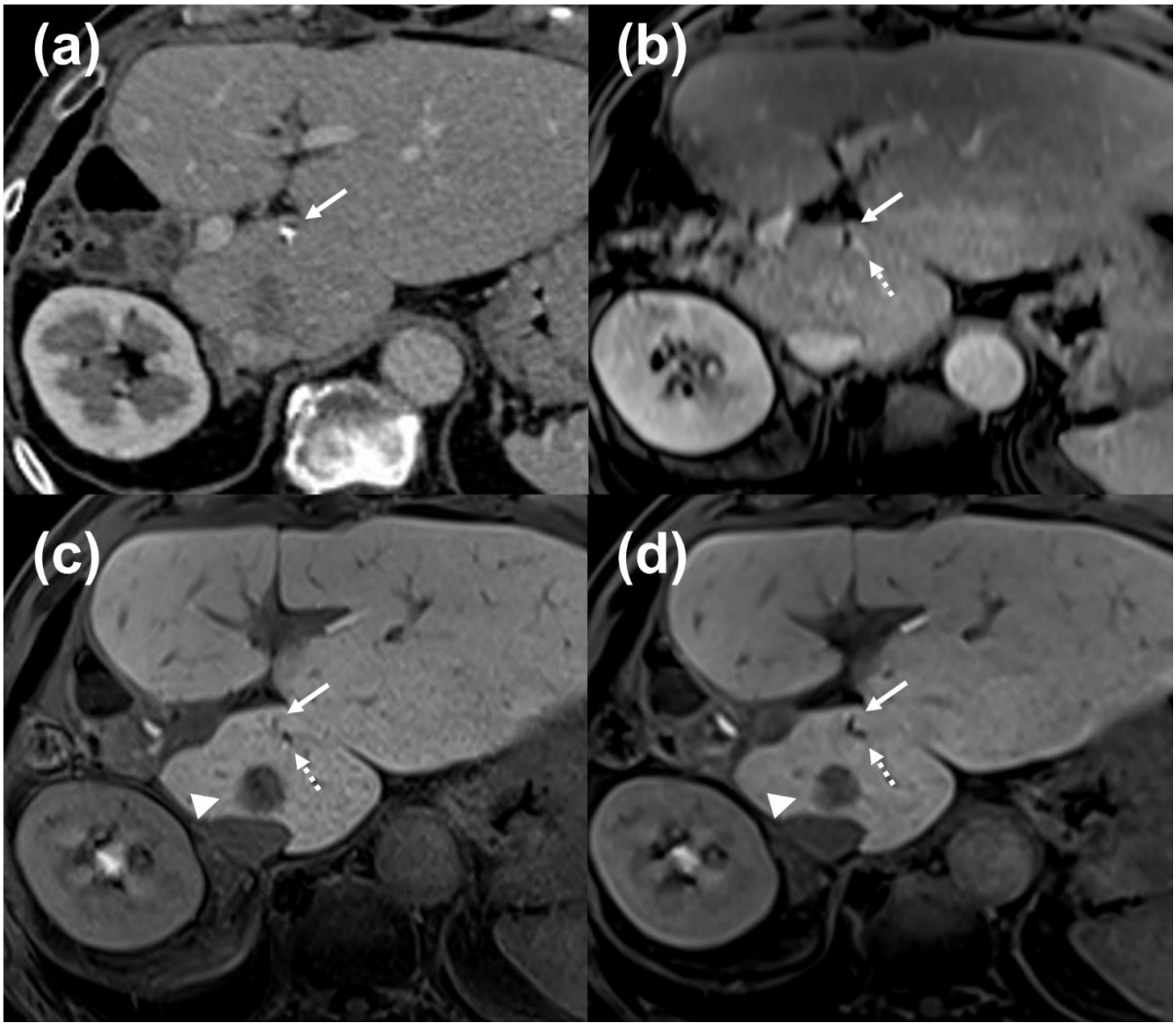

Supplementary Fig. 5. Case 6 of a 72-year-old man with hepatocellular carcinoma: (a) Post-contrast CT shows clear marker visibility. (b) T2*-weighted image shows sufficient marker detection, but the tumor is not distinguishable. (c) Conventional T1-weighted image at the hepatobiliary phase shows excellent tumor delineation, but the marker is unclear. The low signal near the marker (dotted arrow) is a blood vessel, but it may be misidentified as a marker. (d) HYBRID image at the hepatobiliary phase exhibits both clear marker detection and tumor delineation. Arrow: marker; Arrowhead: tumor; Dotted arrow: blood vessel.